



Sensitive and on-site detection of glyphosate based on papain-stabilized fluorescent gold nanoclusters

Chengyi Hong^{1,2} · Sishi Ye¹ · Chenying Dai¹ · Chenyue Wu¹ · Lingling Chen¹ · Zhiyong Huang¹

Received: 30 June 2020 / Revised: 6 September 2020 / Accepted: 11 September 2020 / Published online: 25 September 2020
© Springer-Verlag GmbH Germany, part of Springer Nature 2020

Abstract

Organophosphorus pesticides can prevent or eliminate various pathogenic bacteria, insects, and weeds, and thus they are widely applied in agricultural production. However, illegal use and issues with organophosphorus pesticide residues contribute to global environmental pollution and pose a threat to public health safety. In this study, we developed a sensitive glyphosate (Glyp) fluorescence detection method using papain-stabilized gold nanoclusters (papain-AuNCs) as the fluorescence probe and a tyrosinase (TYR)/dopamine (DA) fluorescence-quenching system. The TYR catalyzed the oxidized conversion of DA into DA chrome, which served as an electron acceptor to quench the fluorescence of papain-AuNCs. However, Glyp inhibited the activity of TYR, thereby preventing DA oxidization and leading to the fluorescence recovery of papain-AuNCs. Under the optimum conditions, the fluorescence intensities of papain-AuNCs exhibited a good linear relationship with the concentration of Glyp in the range of 0.04–0.4 ng·mL⁻¹, and the limit of detection for Glyp was 0.035 ng·mL⁻¹. Furthermore, a paper-based sensor was constructed using the proposed system, which enabled on-site visual and semiquantitative detection of Glyp residues in tap-water samples. Overall, our strategy provides new opportunities for detection of organophosphorus pesticides and evaluation of environmental security.

Keywords Papain · Gold nanoclusters · Glyphosate · Fluorescence detection · Test strip

Introduction

Glyphosate (Glyp) is an organophosphorus pesticide with advantages of high efficacy, wide spectrum, and low cost, and has become one of the most widely used herbicides in the world [1]. Despite its low toxicity and small amounts of residues, its extensive use has produced residues in surface waters in many countries [2]. Moreover, the International Agency for Research on Cancer under the World Health Organization considers Glyp a “probable human carcinogen”

[3]. The intake of Glyp is toxic to human immune and endocrine systems. Therefore, detection of Glyp in the environment is vital and attracts considerable research interest. Common traditional methods of Glyp detection include liquid chromatography/mass spectrometry [4], high-performance liquid chromatography (HPLC) [5], capillary electrophoresis [6], and electrochemical methods [7]. However, these approaches often require large, sophisticated instruments and accompanying high cost, time consumption, and complicated operations, which limits their practical application. Therefore, the development of a fast, sensitive, on-site strategy for Glyp detection is necessary.

Gold nanoclusters (AuNCs) are metal clusters comprising several to hundreds of gold (Au) atoms and are often several nanometers in size [8]. With the advantages of large specific surface area, easy surface modification, and adjustable emission wavelength, AuNCs outperform traditional organic fluorescent molecules in terms of low toxicity, good biocompatibility, and photobleaching resistance [9], leading to their wide application in the detection of biomarkers, heavy-metal ions, small biological molecules, and food pollutants [10]. AuNCs are usually synthesized by the reduction method, where metal

Electronic supplementary material The online version of this article (<https://doi.org/10.1007/s00216-020-02952-7>) contains supplementary material, which is available to authorized users.

✉ Chengyi Hong
cyhong@jmu.edu.cn

¹ College of Food and Biological Engineering, Jimei University, Xiamen 361021, Fujian, China

² College of Food and Biological Engineering, Fujian Provincial Key Laboratory of Food Microbiology and Enzyme Engineering, Jimei University, Xiamen 361021, China

ions and a kind of stabilizer are used as precursors. After the addition of soft reducing agents, metal ions are reduced into metal atoms, which then grow into AuNCs. DNA, amino acids, and proteins are commonly used template molecules [11], among which proteins have good biocompatibility and contain various functional groups (e.g. carboxyl, thiol, and amino groups). These functional groups have a strong affinity toward metals and serve as protecting ligands for AuNC synthesis [11, 12]. In recent studies, a number of proteases including lysozyme [13], horseradish peroxidase [14], and glucose oxidase [15] have been used for the successful synthesis of AuNCs. Au clusters, which are protected by proteins, can also be viewed as conjugates of proteins and Au clusters. They are equipped with dual-function structures while maintaining the functions of proteins, and are thereby suitable for biomedical and environmental applications.

Papain, a kind of cysteine protease with 212 amino acid residues and molecular weight of 23,406 Da, is extensively distributed in the roots, stems, and leaves of pawpaw [16]. Papain is characterized by high temperature resistance, easy hydrolysis, and insensitivity to pH changes, and is thus widely used in food, environmental, and chemical engineering applications [17–19]. In the present study, AuNCs were synthesized using papain as the template and reducing agent under basic pH. A Glyp fluorescence detection method based on a papain-AuNC/tyrosinase (TYR)/dopamine (DA) system was constructed using papain-AuNCs as fluorescence signal molecules. DA can be oxidized to DA chrome, which can quench the fluorescence of papain-AuNCs under TYR catalysis. However, Glyp can inhibit the activity of TYR, thereby preventing DA oxidization and the fluorescence quenching of papain-AuNCs. The proposed method achieves rapid and sensitive detection of Glyp by monitoring fluorescence signals (Scheme 1). Moreover, a fluorescence test paper based on papain-AuNCs was developed and used for the successful detection of Glyp in tap-water samples. Overall, the proposed strategy can serve as a platform for rapid detection of Glyp in environmental water samples.

Experimental

Chemicals and apparatus

Papain, tyrosinase (TYR), and glyphosate (Glyp) were purchased from Sigma-Aldrich (USA). DA was purchased from Shanghai Macklin Biochemical Technology Co., Ltd. (China). Chloroauric acid ($\text{HAuCl}_4 \cdot 4\text{H}_2\text{O}$), soluble starch, D-glucose, D-fructose, glycine, L-tryptophan, L-glutamic acid, bovine serum albumin (BSA), and Tris(hydroxymethyl)methyl aminomethane (Tris) were purchased from Sinopharm Chemical Reagent Co., Ltd. (China). Nylon 66 filter membrane was purchased from

Tianjin Jinteng Experimental Equipment Co., Ltd. (China). All solutions were prepared using ultrapure water (18.2 M Ω -cm, Germany). Fluorescence measurements were performed using an LS55 fluorescence spectrometer (PerkinElmer Ltd., USA). Ultraviolet–visible (UV–Vis) absorption spectra were recorded using a Lambda 265 UV–Vis spectrophotometer (PerkinElmer Ltd., USA). Transmission electron microscopy (TEM) was performed using a field-emission Tecnai G2 F30 microscope at 300 kV. The absolute quantum yield was measured using a steady-state/transient fluorescence spectrometer FLS980 (Edinburgh Instruments, UK). The gold concentration of papain-AuNC solutions was measured by inductively coupled plasma mass spectrometry (Agilent 7700x). Dynamic light scattering (DLS) data were measured using a Zetasizer Nano ZS (Malvern Panalytical, Worcestershire, UK).

Preparation of papain-AuNCs

For the preparation of papain-AuNCs, 1 mL of HAuCl_4 (5 mM) and 1 mL of papain (13 mg·mL⁻¹) were stirred at 37 °C for 10 min. The solution was mixed with 800 μL of NaOH (0.5 mol·L⁻¹), stirred for 2 min, and reacted for 6 h. After the white solution slowly changed to brownish yellow, it was centrifuged with a 3 kDa ultracentrifuge filter at 8000 rpm (~6797 rcf) for 30 min. Tris-HCl buffer was added to obtain papain-AuNC solution (~1.40 mM Au), and pH was adjusted to 7.

Detection of Glyp

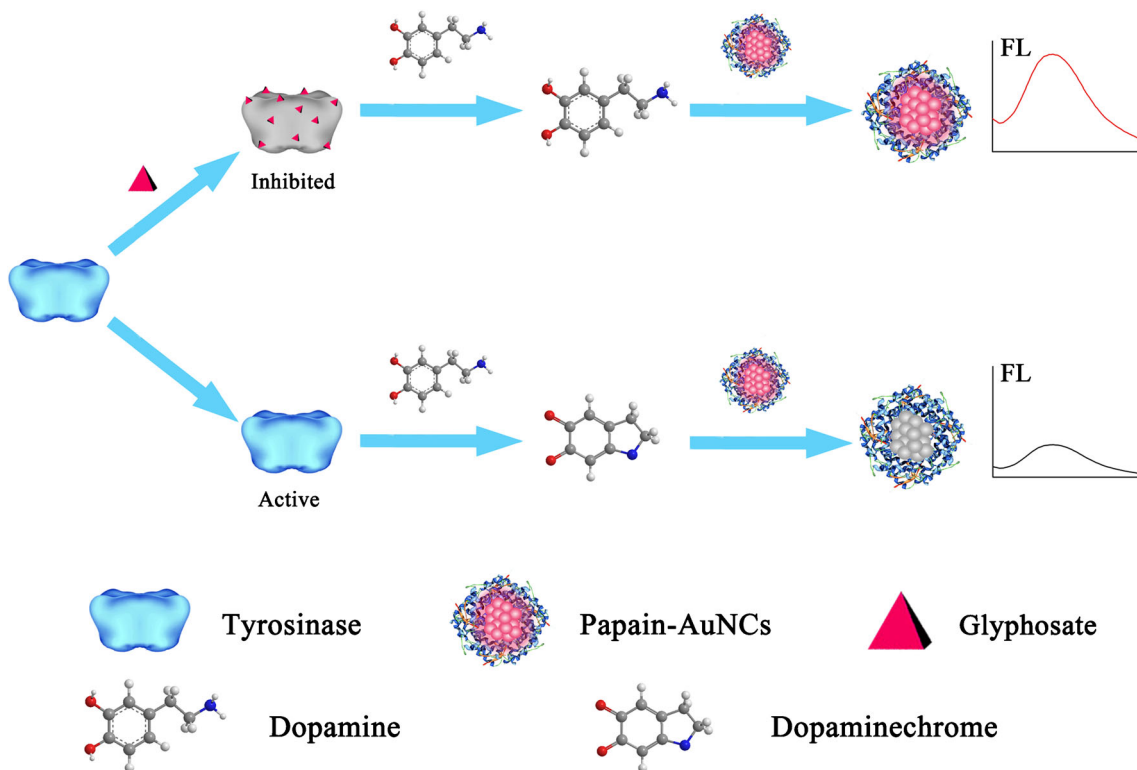
Forty microliters of various concentrations of Glyp (0–10 ng·mL⁻¹) was mixed with 40 μL of TYR (250 U·mL⁻¹), and the solution was shaken for 30 min at 4 °C. After the addition of 80 μL of 10 mM DA, the solution was incubated for 1 h, and 60 μL of papain-AuNCs was added. The above solution was diluted to 400 μL with Tris-HCl buffer and shaken continuously for 10 min. The sample was excited at 470 nm to determine the fluorescence intensity at 650 nm.

Selectivity experiment

For the assay of interfering substances, the TYR and DA system was mixed with 30 ng·mL⁻¹ Na⁺, Mg²⁺, D-glucose, D-fructose, soluble starch, glycine, L-tryptophan, L-glutamic acid, and BSA, respectively, with fivefold concentrations of Glyp. Papain-AuNCs were added to the above solution and shaken for 10 min. The fluorescence intensity was determined as described above.

Glyp detection in real samples

Tap-water samples were selected as real samples for Glyp detection. They were initially filtered through a 0.22- μm



Scheme. 1 Schematic of Glyp detection

membrane and then diluted 10 times using Tris-HCl buffer. A series of Glyp solutions with various concentrations ($0.1, 0.2,$ and $0.4 \text{ ng}\cdot\text{mL}^{-1}$) were added. The fluorescence intensity was determined as described above.

On-site detection of Glyp using a smartphone

Test strips made of nylon filter were immersed in the prepared papain-AuNC solutions for 5 min and dried at room temperature. Then, $100 \mu\text{L}$ of the reaction solution (a mixture of $20 \text{ U}\cdot\text{mL}^{-1}$ TYR, 2 mM DA, and various concentrations of Glyp solutions in tap water) was added dropwise onto the

surface of the test strip. After soaking for 15 min, test strips were wiped clean away from the light and then placed under ultraviolet (UV) light for Glyp detection.

Results and discussion

Optimization of papain-AuNC synthesis conditions

Synthesis conditions for papain-AuNCs were optimized, and the effects of NaOH, papain concentrations, reaction time, and temperature were investigated experimentally. As illustrated

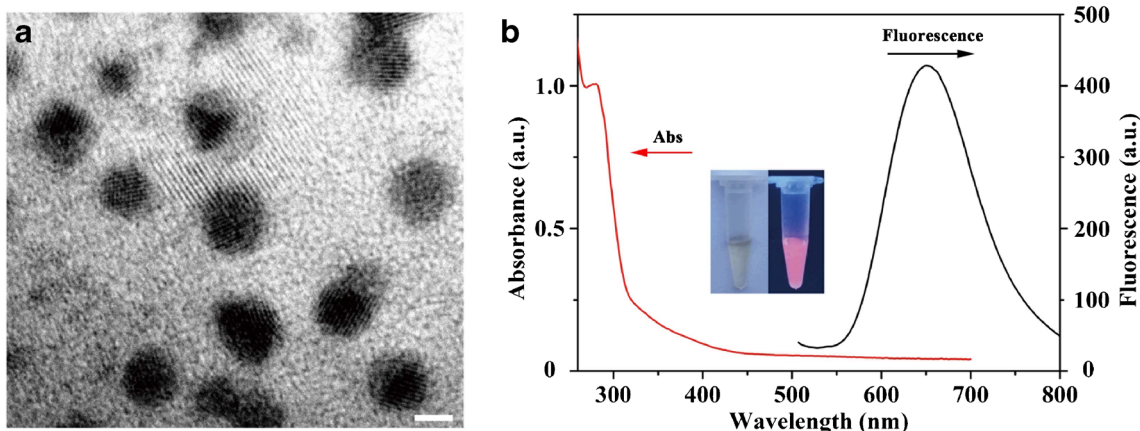


Fig. 1 (a) Transmission electron microscopy (TEM) image of papain-AuNCs. Scale bar: 2 nm. (b) UV-Vis absorption and fluorescence emission spectra of papain-AuNCs. The inset shows the color change of papain-AuNCs with and without UV irradiation

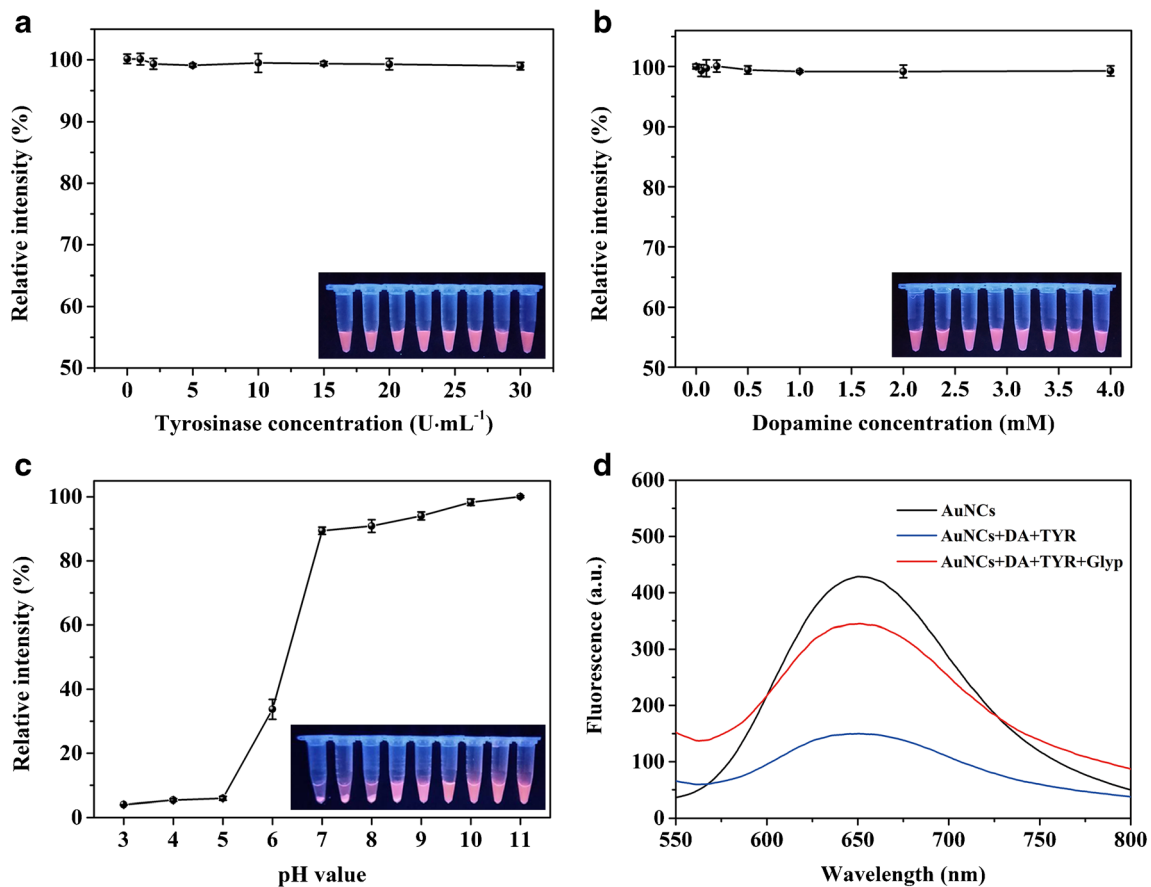


Fig. 2 Fluorescence intensity of papain-AuNCs incubated with different (a) TYR concentrations, (b) DA concentrations, and (c) pH values of the system. The insets in a, b, and c show the fluorescence color of papain-AuNCs with UV irradiation. (d) Fluorescence intensity of different

systems: papain-AuNCs (black line), papain-AuNCs+TYR + DA (blue line), and papain-AuNCs+TYR + DA + Glyp (red line). The illustrated error bars represent the standard deviation of three repetitive measurements

in Fig. S1A (see Electronic Supplementary Material, ESM), the highest fluorescence intensity of the papain-AuNCs was observed when the NaOH concentration was 0.5 M. As shown

in Fig. S1B (see ESM), the fluorescence intensity of papain-AuNCs increased with the increasing concentration of papain until the fluorescence signal reached a plateau at 13 mg·mL⁻¹.

Table 1 Comparison of various methods for Glyp determination

Method	Linear range (ng mL ⁻¹)	LOD (ng mL ⁻¹)	Real sample	Reference
Photoelectrochemical	(1.0 × 10 ⁻¹⁰ –1.0 × 10 ⁻³)	30 pM	–	[23]
Fluorescence	1.69 × 10 ⁻² –1.69 × 10 ⁵ (0.025–2.5 μg·mL ⁻¹)	5.07 × 10 ⁻³ 12	Cereal	[24]
Fluorescence	25–2500 (0.02–2.0 μg·kg ⁻¹)	(9.8 ng kg ⁻¹) 9.8 × 10 ⁻³	Apple	[25]
Fluorescence	0.02–2.0 (0.02–1.5 μg·mL ⁻¹)	18.30	Water	[26]
Colorimetric	20–1.5 × 10 ³ (0.002–0.01 ppm)	(0.67 ppb)	Water	[27]
Colorimetric	2–100 (2–200 μM)	0.67 (1 μM)	Water	[28]
Colorimetric	338–33,800 (0.01–0.75 nM)	169 (1.94 pM)	Water	[29]
Fluorescence	1.69 × 10 ⁻³ –0.13 0.04–0.4	3.28 × 10 ⁻⁴ 0.035	Water	This work

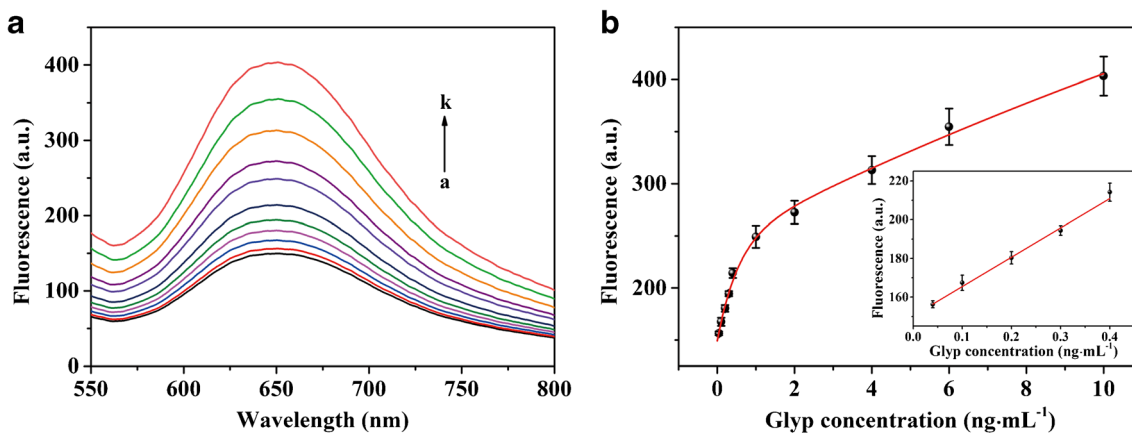


Fig. 3 (A) Fluorescence emission spectra of the papain-AuNC/TYR/DA system in the presence of different concentrations of Glyp (a) blank and (b–k) 0.04, 0.1, 0.2, 0.3, 0.4, 1, 2, 4, 6, and 10 ng·mL⁻¹, respectively. (B)

The standard curve of Glyp. The inset shows the linear fitting of the fluorescence intensity at 650 nm versus Glyp concentrations

Therefore, 13 mg·mL⁻¹ was selected as the optimum papain concentration for further experiments. As presented in Fig. S1C and S1D (see ESM), the highest fluorescence intensity was observed at a reaction time and temperature of 6 h and 37 °C, respectively.

Characterization of papain-AuNCs

The morphology of papain-AuNCs was first characterized by transmission electron microscopy (TEM). Papain-AuNCs, with an average diameter of about 4 nm, were well dispersed (Fig. 1A and ESM Fig. S2A). The small particle size may be attributed to the stabilization provided by the papain template. The optical properties of papain-AuNCs were then examined by fluorescence spectroscopy, which revealed maximum emission wavelength of 650 nm (Fig. 1B, black line). In addition, the color of papain-AuNCs illuminated by a fluorescent lamp was compared with that illuminated by a 365-nm UV lamp. Papain-AuNCs showed pink fluorescence under the

irradiation of the UV lamp (Fig. 1B, inset), with absolute quantum yield of 12.40%, using BaSO₄ as a standard [20]. The absorption spectrum of the papain-AuNCs displayed strong absorption in the UV region, with a peak at around 280 nm (Fig. 1B, red line). X-ray spectroscopy analysis of the papain-AuNCs revealed the presence of peaks for Au 4f_{7/2} at 83.8 eV and for Au 4f_{5/2} at 87.4 eV, respectively (ESM Fig. S2B). Finally, papain-AuNCs exhibited good photostability and maintained approximately 96% of initial fluorescence intensity after continuous irradiation for 60 min (ESM Fig. S3). Taken together, these results suggested that papain-AuNCs were successfully synthesized.

Feasibility of the experiments

The effects of different concentrations of DA and TYR on the fluorescence intensity of papain-AuNCs are shown in Fig. 2a and b. The results indicated that the fluorescence intensity of the AuNCs did not change significantly within

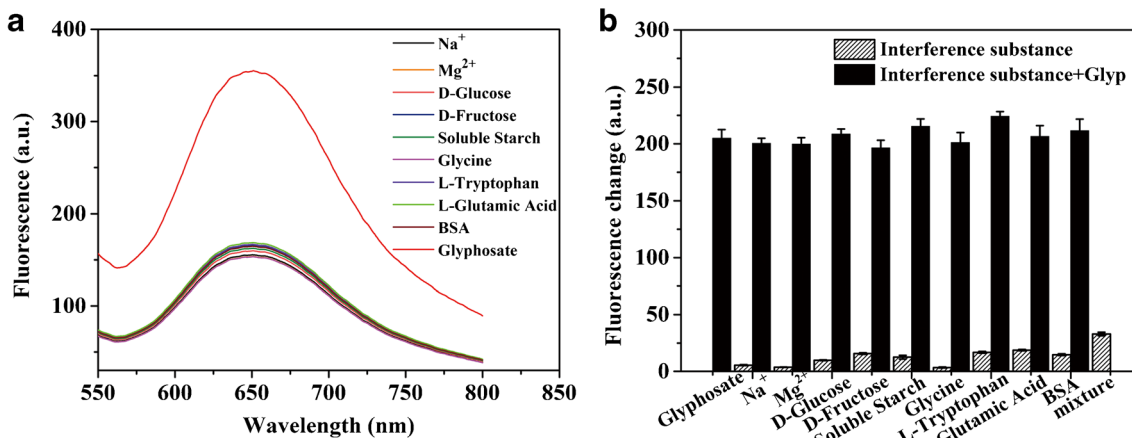


Fig. 4 Selectivity of the method. (a) Fluorescence emission spectra of papain-AuNC/TYR/DA system in the presence of different contents. (b) Fluorescence change of papain-AuNC/TYR/DA system with Glyp

(6 ng·mL⁻¹) and interfering substances (30 ng·mL⁻¹), including Na⁺, Mg²⁺, D-glucose, D-fructose, soluble starch, glycine, L-tryptophan, L-glutamic acid, and BSA

Table 2 Recovery analysis of Glyp in tap-water samples

Tap-water samples	Glyp added (ng·mL ⁻¹)	Glyp recovered (ng·mL ⁻¹)	Recovery (%)	RSD (<i>n</i> = 3, %)
Sample 1	0.1	0.114 ± 0.005	114	4.39
	0.2	0.217 ± 0.008	108.5	3.69
	0.4	0.405 ± 0.012	101.3	2.96
Sample 2	0.1	0.118 ± 0.007	118	5.93
	0.2	0.197 ± 0.010	98.5	5.08
	0.4	0.413 ± 0.017	103.3	4.12
Sample 3	0.1	0.112 ± 0.004	112	3.57
	0.2	0.218 ± 0.008	109	3.67
	0.4	0.389 ± 0.013	97.3	3.34

a DA concentration range of 0–4 mM and TYR concentration of 0–30.0 U·mL⁻¹. As shown in Fig. 2C, the fluorescence signal of the papain-AuNCs increased with increasing pH. Neutral pH was set as 7 because of the polymerization of DA under an alkaline environment [21]. The fluorescence intensity of the papain-AuNCs + TYR + DA + Glyp system (red line in Fig. 2D) increased significantly compared with that of the papain-AuNCs + TYR + DA system (blue line in Fig. 2D), indicating that Glyp inhibited TYR activity to prevent DA oxidation and the quenching of papain-AuNC fluorescence.

Optimization of detection conditions

To determine the optimum conditions for Glyp detection, concentrations of TYR and DA were optimized. As displayed in Fig. S4A (see ESM), with the increasing concentration of TYR, the fluorescence intensity of papain-AuNCs decreased, and the quenching effect remained unchanged when the concentration of TYR reached 25 U·mL⁻¹. Considering the inhibition effect of high concentrations of TYR [22], 25 U·mL⁻¹ was selected as the optimal TYR concentration. Fig. S4B (see ESM) showed that when TYR (25 U·mL⁻¹) reacted with different concentrations of DA (0.2–5 mM), the fluorescence intensity of AuNCs did not change when the concentration of DA reached 2 mM. Therefore, 2 mM DA was selected.

Table 3 Comparison of the proposed method with the standard HPLC assay

Methods	Glyp added (ng·mL ⁻¹)	Glyp recovered (ng·mL ⁻¹)	Recovery (%)
This work	0.1	0.114 ± 0.005	114
	0.2	0.217 ± 0.008	108.5
	0.4	0.405 ± 0.012	101.3
HPLC	0.1	0.108 ± 0.004	108
	0.2	0.198 ± 0.006	99.0
	0.4	0.428 ± 0.010	107

Fluorescence detection of Glyp

Glyp inhibited the activity of TYR to prevent the formation of DA chrome, thereby enhancing the fluorescence intensity. The fluorescence intensity of the reaction system at 650 nm was enhanced with increasing Glyp concentrations (0.04–10 ng·mL⁻¹) under optimum reaction conditions (Fig. 3A). As shown in Fig. 3B, a good linear relationship between fluorescence intensity and Glyp concentrations (0.04–0.4 ng·mL⁻¹) was established. The linear equation was $F = 151.5 C_{(\text{Glyp})} + 150.3$ with a correlation coefficient $R^2 = 0.9944$, and the limit of detection (LOD) calculated by three times the standard deviation was 0.035 ng·mL⁻¹. As listed in Table 1, the proposed method had a relatively lower LOD than those of previously reported fluorescence-based detection methods.

Selectivity experiments

The selectivity of the papain-AuNC/TYR/DA system was evaluated by introducing common co-existing substances and interfering substances, including Na⁺, Mg²⁺, D-glucose, D-fructose, soluble starch, glycine, L-tryptophan, L-glutamic acid, and BSA. As illustrated in Fig. 4A, the fluorescence recovery induced by Glyp was not influenced by other interfering substances, indicating that the papain-AuNC/TYR/DA system maintained high selectivity to Glyp pesticides among

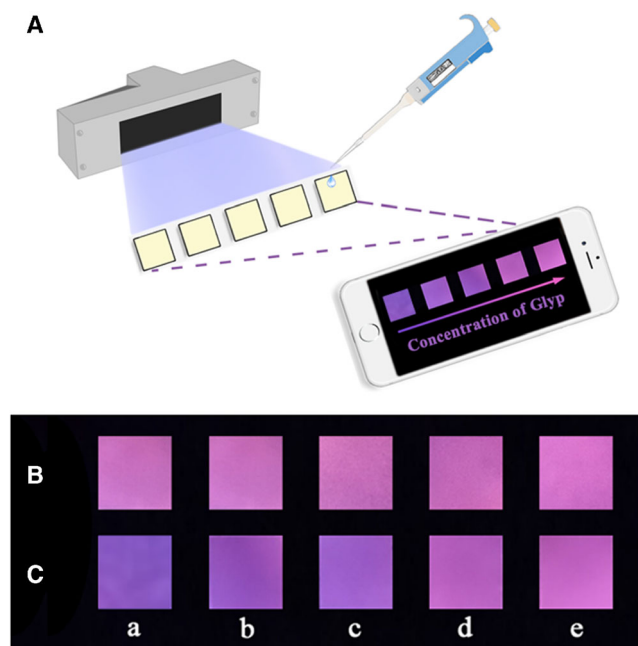


Fig. 5 (A) Scheme of the visual detection of Glyp using test strips under UV illumination. (B) The standard fluorescence card of test strips. (C) Test strips incubated with different Glyp concentrations (a: blank; b–e: 2.0, 5.0, 25.0, and 50.0 $\text{ng}\cdot\text{mL}^{-1}$, respectively)

different interfering substances and held the potential for practical use of real samples (Fig. 4B).

Real sample detection

To verify the practical feasibility of the papain-AuNC/TYR/DA system, we explored the detection of Glyp in tap-water samples based on the standard addition method. A series of Glyp concentrations (0.1, 0.2, and 0.4 $\text{ng}\cdot\text{mL}^{-1}$) at equal volumes were added into tap-water samples, and Glyp was measured using the proposed method. As listed in Table 2, sample recovery ranging from 97.3% to 118% was obtained. Moreover, the detected Glyp levels in tap-water samples agreed with those using HPLC (Table 3), indicating that the method can be used for practical applications with satisfactory accuracy.

On-site detection of Glyp using a smartphone

To further expand the practical use of our method, a simple and portable test strip based on papain-AuNCs was constructed (Fig. 5A). The AuNC test strip was developed by dispersing papain-AuNC solution onto the surface of the test strip. Pale pink fluorescence of the test strip was observed under a 365-nm UV lamp (Fig. 5B). Afterwards, a series of tap-water samples with different concentrations of Glyp (2.0, 5.0, 25.0, and 50.0 $\text{ng}\cdot\text{mL}^{-1}$) and TYR/DA were added dropwise onto the test strip and incubated for 15 min. By comparison with the standard fluorescence card

(Fig. 5B), the concentration of Glyp was calculated according to the fluorescence color, thereby achieving visual and semiquantitative detection. It was observed that the color changed from purple to pink with increasing Glyp concentration (2.0, 5.0, 25.0, and 50.0 $\text{ng}\cdot\text{mL}^{-1}$) (Fig. 5C). Glyp with low concentrations resulted in purple fluorescence [Fig. 5C (a–c)], while high concentrations led to pink fluorescence [Fig. 5C (d and e)]. Furthermore, quantitative analysis was achieved by capturing test strips with a smartphone and calculated using ImageJ software (ESM Fig. S5). This software split the original RGB photo into three primary-color image channels (red, blue, and green), and mean gray values were selected to represent the corresponding fluorescence intensity. As shown in Fig. S6 (see ESM), the mean gray values in the red channel were proportional to the logarithm of Glyp concentrations in the range of 2.0–50.0 $\text{ng}\cdot\text{mL}^{-1}$. These results demonstrated that the combination of test strips with a smartphone offered a highly powerful and portable platform for cost-effective and convenient on-site Glyp detection.

Conclusion

We developed a sensitive and on-site method for Glyp detection based on the fluorescence change of papain-AuNCs and the fluorescence-quenching system of TYR/DA. The formation of DA chrome catalyzed by TYR quenched the fluorescence of papain-AuNCs. However, Glyp inhibited the activity of TYR, thereby preventing DA oxidation and leading to the fluorescence recovery of papain-AuNCs. Overall, the papain-AuNC/TYR/DA system provides a novel platform for Glyp detection. Under optimum conditions, linear calibration was obtained within the Glyp concentration range of 0.04–0.4 $\text{ng}\cdot\text{mL}^{-1}$, and the LOD was 0.035 $\text{ng}\cdot\text{mL}^{-1}$. Moreover, the approach was applied for the detection of Glyp in tap-water samples, with results comparable to those using the HPLC method. We further constructed an AuNC-based test strip for on-site visual Glyp detection in tap water using a smartphone and ImageJ software. Taken together, the proposed method is environmentally friendly, easy to prepare, and cost-effective, holding the potential for practical use in environmental aqueous solution and biological sensing processes.

Acknowledgements This work was supported by the National Natural Science Foundation of China (21804050) and the Natural Science Foundation of Fujian Province of China (2019 J05098).

Compliance with ethical standards

Conflict of interest The authors declare no conflict of interest.

References

- Valle AL, Mello FCC, Alves-Balvedi RP, Rodrigues LP, Goulart L. Glyphosate detection: methods, needs and challenges. *Environ Chem Lett*. 2019;17(1):291–317. <https://doi.org/10.1007/s10311-018-0789-5>.
- Singh S, Kumar V, Datta S, Wani AB, Dhanjal DS, Romero R, et al. Glyphosate uptake, translocation, resistance emergence in crops, analytical monitoring, toxicity and degradation: a review. *Environ Chem Lett*. 2020;18:1–40. <https://doi.org/10.1007/s10311-020-00969-z>.
- Williams GM, Aardema M, Acquavella J, Berry BC, Brusick D, Burns MM, et al. A review of the carcinogenic potential of glyphosate by four independent expert panels and comparison to the IARC assessment. *Crit Rev Toxicol*. 2016;46(sup1):3–20. <https://doi.org/10.1080/10408444.2016.1214677>.
- Lee EA, Zimmerman LR, Bhullar BS, Thurman EM. Linker-assisted immunoassay and liquid chromatography/mass spectrometry for the analysis of glyphosate. *Anal Chem*. 2002;74(19):4937–43. <https://doi.org/10.1021/ac020208y>.
- Bernal J, Bernal JL, Martín MT, Nozal MJ, Anadón A, Martínez-Larranaga MR, et al. Development and validation of a liquid chromatography–fluorescence–mass spectrometry method to measure glyphosate and aminomethylphosphonic acid in rat plasma. *J Chromatogr B*. 2010;878(31):3290–6. <https://doi.org/10.1016/j.jchromb.2010.10.013>.
- Corbera M, Hidalgo M, Salvado V, Wiczorek PP. Determination of glyphosate and aminomethylphosphonic acid in natural water using the capillary electrophoresis combined with enrichment step. *Anal Chim Acta*. 2005;540(1):3–7. <https://doi.org/10.1016/j.aca.2004.12.028>.
- Cao Y, Wang L, Shen C, Wang C, Hu X, Wang G. An electrochemical sensor on the hierarchically porous cu-BTC MOF platform for glyphosate determination. *Sens Actuators B Chem*. 2019;283:487–94. <https://doi.org/10.1016/j.snb.2018.12.064>.
- Alex S, Tiwari A. Functionalized gold nanoparticles: synthesis, properties and applications—a review. *J Nanosci Nanotechnol*. 2015;15(3):1869–94. <https://doi.org/10.1166/jnm.2015.9718>.
- Shang L, Xu J, Nienhaus GU. Recent advances in synthesizing metal nanocluster-based nanocomposites for application in sensing, imaging and catalysis. *Nano Today*. 2019;28:100767. <https://doi.org/10.1016/j.nantod.2019.100767>.
- Cui M, Zhao Y, Song Q. Synthesis, optical properties and applications of ultra-small luminescent gold nanoclusters. *TrAC Trends Anal Chem*. 2014;57:73–82. <https://doi.org/10.1016/j.trac.2014.02.005>.
- Song XR, Goswami N, Yang HH, Xie J. Functionalization of metal nanoclusters for biomedical applications. *Analyst*. 2016;141(11):3126–40. <https://doi.org/10.1039/C6AN00773B>.
- Xie J, Zheng Y, Ying JY. Protein-directed synthesis of highly fluorescent gold nanoclusters. *J Am Chem Soc*. 2009;131(3):888–9. <https://doi.org/10.1021/ja806804u>.
- Lin YH, Tseng WL. Ultrasensitive sensing of Hg²⁺ and CH₃Hg⁺ based on the fluorescence quenching of lysozyme type VI-stabilized gold nanoclusters. *Anal Chem*. 2010;82(22):9194–200. <https://doi.org/10.1021/ac101427y>.
- Wen F, Dong Y, Feng L, Wang S, Zhang S, Zhang X. Horseradish peroxidase functionalized fluorescent gold nanoclusters for hydrogen peroxide sensing. *Anal Chem*. 2011;83(4):1193–6. <https://doi.org/10.1021/ac1031447>.
- Xia X, Long Y, Wang J. Glucose oxidase-functionalized fluorescent gold nanoclusters as probes for glucose. *Anal Chim Acta*. 2013;772:81–6. <https://doi.org/10.1016/j.aca.2013.02.025>.
- Chen Y, Wang Y, Wang C, Li W, Zhou H, Jiao H, et al. Papain-directed synthesis of luminescent gold nanoclusters and the sensitive detection of Cu²⁺. *J Colloid Interf Sci*. 2013;396:63–8. <https://doi.org/10.1016/j.jcis.2013.01.031>.
- Liu S, Höldrich M, Sievers-Engler A, Horak J, Lämmerhofer M. Papain-functionalized gold nanoparticles as heterogeneous biocatalyst for bioanalysis and biopharmaceuticals analysis. *Anal Chim Acta*. 2017;963:33–43. <https://doi.org/10.1016/j.aca.2017.02.009>.
- Ardila-Fierro KJ, Crawford DE, Körner A, James SL, Bolm C, Hernández JG. Papain-catalysed mechanochemical synthesis of oligopeptides by milling and twin-screw extrusion: application in the Juliá–Colonna enantioselective epoxidation. *Green Chem*. 2018;20(6):1262–9. <https://doi.org/10.1039/C7GC03205F>.
- Atacan K, Özacar M, Özacar M. Investigation of antibacterial properties of novel papain immobilized on tannic acid modified ag/CuFe₂O₄ magnetic nanoparticles. *Int J Biol Macromol*. 2018;109:720–31. <https://doi.org/10.1016/j.ijbiomac.2017.12.066>.
- Li Q, Wu X, Huang X, Deng Y, Chen N, Jiang D, et al. Tailoring the fluorescence of AIE-active metal–organic frameworks for aqueous sensing of metal ions. *ACS Appl Mater Interfaces*. 2018;10(4):3801–9. <https://doi.org/10.1021/acsami.7b17762>.
- Lin LS, Cong ZX, Cao JB, Ke KM, Peng QL, Gao J, et al. Multifunctional Fe₃O₄@ polydopamine core–shell nanocomposites for intracellular mRNA detection and imaging-guided photothermal therapy. *ACS Nano*. 2014;8(4):3876–83. <https://doi.org/10.1021/nm500722y>.
- Yan X, Li H, Hu T, Su X. A novel fluorimetric sensing platform for highly sensitive detection of organophosphorus pesticides by using egg white-encapsulated gold nanoclusters. *Biosens Bioelectron*. 2017;91:232–7. <https://doi.org/10.1016/j.bios.2016.11.058>.
- Li Y, Zhang S, Zhang Q, Xu G, Dai H, Lin Y. Binding-induced internal-displacement of signal-on photoelectrochemical response: a glyphosate detection platform based on graphitic carbon nitride. *Sens Actuators B Chem*. 2016;224:798–804. <https://doi.org/10.1016/j.snb.2015.10.111>.
- Wang L, Bi Y, Hou J, Li H, Xu Y, Wang B, et al. Facile, green and clean one-step synthesis of carbon dots from wool: application as a sensor for glyphosate detection based on the inner filter effect. *Talanta*. 2016;160:268–75. <https://doi.org/10.1016/j.talanta.2016.07.020>.
- Guo J, Zhang Y, Luo Y, Shen F, Sun C. Efficient fluorescence resonance energy transfer between oppositely charged CdTe quantum dots and gold nanoparticles for turn-on fluorescence detection of glyphosate. *Talanta*. 2014;125:385–92. <https://doi.org/10.1016/j.talanta.2014.03.033>.
- Wang X, Sakinati M, Yang Y, Ma Y, Yang M, Luo H, et al. The construction of a CND/Cu²⁺ fluorescence sensing system for the ultrasensitive detection of glyphosate. *Anal Methods*. 2020;12(4):520–7. <https://doi.org/10.1039/C9AY02303H>.
- Chang YC, Lin YS, Xiao GT, Chiu TC, Hu CC. A highly selective and sensitive nanosensor for the detection of glyphosate. *Talanta*. 2016;161:94–8. <https://doi.org/10.1016/j.talanta.2016.08.029>.
- Chang Y, Zhang Z, Hao J, Yang W, Tang J. A simple label free colorimetric method for glyphosate detection based on the inhibition of peroxidase-like activity of cu (II). *Sens Actuators B Chem*. 2016;228:410–5. <https://doi.org/10.1016/j.snb.2016.01.048>.
- Bala R, Dhingra S, Kumar M, Bansal K, Mittal S, Sharma RK, et al. Detection of organophosphorus pesticide–malathion in environmental samples using peptide and aptamer based nanoprobe. *Chem Eng J*. 2017;311:111–6. <https://doi.org/10.1016/j.cej.2016.11.070>.

Publisher's note Springer Nature remains neutral with regard to jurisdictional claims in published maps and institutional affiliations.